Chapter 4
Photocatalysts for Reduction of Molecular Oxygen to Hydrogen Peroxide

Daniil A. Lukyanov and Alexander S. Konev

Abstract A brief overview of compounds and materials exhibiting photocatalytic activity in reduction of molecular oxygen to hydrogen peroxide is given with focus on comparison of the performance of reported photocatalysts. The photocatalysts are treated in two major classes: the inorganic semiconductors, which include various metal oxides and chalcogenides, and carbon-based photocatalysts, which cover a wide range of carbon-based compounds from small organic molecules to graphene materials. The review is preceded by brief description of analytical techniques available for quantification of hydrogen peroxide formation.

4.1 Introduction

The oxygen reduction reaction (ORR) may result in the formation of two stable oxygen species. Formal two-electron reduction affords hydrogen peroxide, while the four-electron process produces water. The product of the two-electron reduction, H_2O_2, represents a low-hazardous energy-rich compound, which can serve either as energy storage material [1] or as a "green" and strong oxidant, widely used in chemical industries. Hydrogen peroxide is mostly produced via the anthraquinone process of indirect oxygen hydrogenation developed by BASF [2]. In this process, 2-ethylanthraquinone is subjected to palladium-catalyzed hydrogenation to form the corresponding hydroquinone, which then selectively reduces oxygen to hydrogen peroxide. The anthraquinone process, in addition to hazardous reagents and expensive catalyst, consumes a large amount of energy for the hydrogenation reaction. An appealing new approach to H_2O_2 production exploits the solar energy in a photocatalytic oxygen reduction.

For the first time, the photochemical formation of hydrogen peroxide upon exposure to light of ZnO particles in the presence of oxidizable material was published

D. A. Lukyanov (✉) · A. S. Konev
Institute of Chemistry, Saint Petersburg State University, Saint Petersburg 199034, Russia

A. S. Konev
e-mail: a.konev@spbu.ru

K. Yamanouchi et al. (eds.), *Progress in Photon Science*, Springer Series in Chemical Physics 125, https://doi.org/10.1007/978-3-030-77646-6_4

by Baur and Neuweiler in 1927 [3]. Later, the photocatalytic formation of hydrogen peroxide was observed on various heterogeneous and homogeneous photocatalysts.

In the middle of the previous century, natural photocatalytic systems for two-electron ORR were discovered. In 1951, Alan Mehler showed that molecular oxygen is reduced in chloroplasts to hydrogen peroxide under the action of sunlight [4]. The reaction proceeded in two steps—the one-electron reduction of molecular oxygen to superoxide anion by ferridoxine followed by its disproportionation to oxygen and hydrogen peroxide under the action of superoxide dismutase.

In the recent decades, major advances have been achieved in the development of photocatalysts for ORR. A great effort was made on the way to improve the photocatalytic performance of the metal oxide semiconductors. A number of the next generation semiconductor catalysts based on 2D and 3D nanomaterials was developed, including graphene derivatives, graphene-like carbon nitride, etc. Molecular photocatalysts for ORR were found amongst organic and metal-organic molecules. Several reviews were devoted to the fundamentals and performance of organic [5, 6], inorganic [7, 8] and nanostructured [9] ORR photocatalysts. In the present overview, we aim to cover and compare these types of photocatalysts.

4.1.1 Oxygen Reduction Reactions

The main redox reactions involving molecular oxygen and related particles are shown in Latimer diagram (Fig. 4.1).

Standard electrode potential of the two-electron process of interest (4.1) is 0.695 V. The photocatalytic ORR may employ water as an electron donor in a so-called non-sacrificial process, or consume any additional reductant as a sacrificial electron donor. Depending on the nature of the sacrificial donor, reaction may be either exothermic or endothermic. The non-sacrificial ORR reaction, described by 4.6, is endothermic with ΔG of ca. 100 kJ per mole H_2O_2, thus requiring an external energy source (light with $\lambda < 1100$ nm or external bias), but most of the sacrificial donors shift the ORR to the exothermic region.

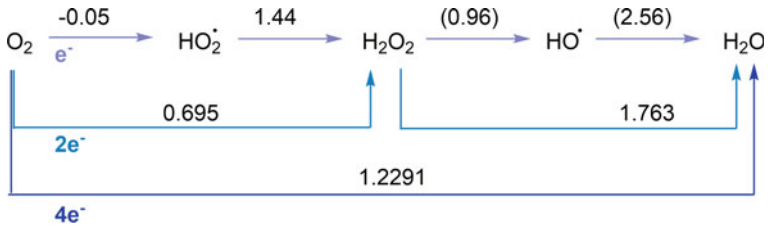

Fig. 4.1 Latimer diagram of oxygen. Standard redox potentials are reported in V versus SHE. The number of digits reflects the accuracy of measurements. Estimated values are given in parentheses. Data taken from [10]

$$O_2 + 2H^+ \xrightarrow{2e} H_2O_2 \tag{4.1}$$

$$O_2 \xrightarrow{e} O_2^{\cdot -} \tag{4.2}$$

$$2O_2^{\cdot -} + 2H^+ \rightarrow H_2O_2 + O_2 \tag{4.3}$$

$$H_2O_2 + H^+ \xrightarrow{e} HO^{\cdot} + H_2O \tag{4.4}$$

$$2OH^{\cdot} \rightarrow H_2O_2 \tag{4.5}$$

$$O_2 + 2H_2O \rightarrow 2H_2O_2 \tag{4.6}$$

However, the kinetics of the direct ORR is sluggish for both two-electron and four-electron processes, even strong reducing agents are often unable to reduce oxygen molecule without a catalyst. Photocatalysis facilitates this reaction, generally via one of two processes that potentially lead to the formation of hydrogen peroxide. The first process is the one-electron reduction of oxygen to the superoxide anion (4.2) with standard potential of − 0.046 V. The superoxide anion can spontaneously or catalytically dismutate in the presence of protons (4.3). The second process, occurring mainly on the surface of a heterogeneous catalyst, is the reduction of the hydrogen peroxide to afford hydroxyl radical (4.4) with a potential of 0.96 V. Hydroxyl radical may then recombine according to (4.5). In addition, catalyst-specific reduction pathways are known, mostly for molecular catalysts.

In practice, the two-electron ORR is accompanied by decomposition of the target product, hydrogen peroxide. It was shown that at room temperature, hydrogen peroxide decomposes quickly enough to affect the results of the photocatalytic synthesis, but when the temperature drops below + 14 °C the decomposition rate in the absence of impurities catalyzing the reaction becomes negligible [11]. In addition, the photocatalyst itself may catalyze the decomposition of H_2O_2, either as a dark process or under illumination. As a result, a plateau of H_2O_2 concentration corresponding to quasi-stationary concentration, $[H_2O_2]_{QS}$, is often observed when the decomposition rate of the hydrogen peroxide reaches its formation rate. Another problem, is the degradation of the ORR photocatalysts over the time of operation, which results in decreasing of the H_2O_2 concentration after it reaches the maximum.

4.1.2 Evaluation of Photocatalysts

Based on the aggregate state, ORR photocatalysts may be divided into solid state and molecular catalysts. Solid state photocatalysts are continuous solids with two-band electronic structure typical of semiconductors. Photoexcitation from the valence band

promotes an electron to the conduction band, where the electron may traverse to an oxygen adsorbed on the surface and reduces the oxygen molecule. Abstraction of an electron from a reductant to the valence band of the photocatalyst completes the photocatalytic cycle. Molecular photocatalysts are single molecules with discrete levels of electronic energy. The catalytic cycle in this case includes photoexcitation of the catalyst, abstraction of an electron from the photoexcited catalyst molecule by oxygen and reduction of the oxidized catalyst by a sacrificial electron donor. The mechanism of catalytic action is thus similar in both cases. However, the difference in the aggregate state leads to a difference in possible operation modes of the photocatalytic process: the solid state photocatalysts inevitably lead to a heterogenous reaction mode, while molecular photocatalysts can operate in a homogenous mode.

The photocatalytic performance of a catalyst in two-electron ORR is estimated using different indicators, depending on the catalyst type. Turnover number (TON) and turnover frequency (TOF) are used for molecular photocatalysts, while for solid state catalysts H_2O_2 production per 1 g of catalyst and H_2O_2 production per 1 g of catalyst in 1 s might be used instead of TON and TOF respectively. In case of a sacrificial ORR, the conversion of the sacrificial donor, the yield of H_2O_2, and selectivity are also used to characterize the photocatalytic process. Due to the possible decomposition of H_2O_2, the maximal achievable concentration of H_2O_2 is a good indicator for comparison of different photocatalytic systems. Wavelength specific quantum yields for the ORR photocatalysts or more practical solar light utilization efficiencies are measured to determine the light utilization performance of the catalyst. The coulombic efficiency, two- versus four-electron ORR selectivity, and external bias value should also be determined for photoelectrocatalysts.

To determine the H_2O_2 content in the reaction mixture, a large variety of analytical methods are employed. Iodometric titration [12], which was employed in early studies, is quite time-consuming and is rarely used now due to the low selectivity and low sensitivity. More useful are photometric methods such as iodide photometric [13], cobalt peroxide [14] and peroxotitanyl assays [15]. Iodide and cobalt peroxide assays employ photometry using ultraviolet light at the wavelength below 300 nm, which is absorbed by many sacrificial donor additives and organic solvents, interfering thus with the results of analysis. In a titanyl assay, an absorption at 400 nm is measured, which is more suitable for complex systems. Besides, formation of peroxy compounds of metals is not influenced by other oxidants like dissolved oxygen, which makes it a more selective method.

The most selective and sensitive photometric determination of hydrogen peroxide is achieved with horse radish peroxidase assay [16]. The use of peroxidase enzyme secures the selectivity of H_2O_2 determination in the presence of any oxidants, and the working wavelength is determined by the peroxidase substrate, which may be chosen from the large variety of commercial compounds. However, the possible interferences from sacrificial donors should be studied in each case. Chemiluminescent luminol-peroxidase assays for hydrogen peroxide delivers even higher sensitivity, providing the quantitative determination with detection limit below 100 nM [17].

Many electrochemical sensors for the hydrogen peroxide determination are developed, including the enzymatic electrodes [18]. The chromatographic determination

of H_2O_2 may be performed directly using HPLC with an ion exchange column [19] or by analyzing the products of the derivatization [20]. Direct GC determination of hydrogen peroxide is impossible due to thermal decomposition, but the headspace determination of the oxygen released by its catalytic decomposition is possible [21].

Mechanistic studies of the photocatalytic ORR may be performed by different techniques. For model studies, organic dyes are widely used as sacrificial electron donors, since their concentration may be easily monitored photometrically. However, the dye degradation assays do not provide direct information on the oxygen reduction, so the kinetic curves for hydrogen peroxide formation and/or oxygen uptake should be obtained for more detailed investigation. In case of photoelectrocatalysis, the reaction current may also be used.

The two-electron ORR is often accompanied with an intermediate formation of reactive oxygen species (ROS), including superoxide radicals, hydroxyl radical and singlet oxygen. The detection of radical ROS's may be done using EPR technique or radical scavengers. In case of solid state catalysts, the surface bound radical particles may be determined by FTIR and/or Raman spectroscopy. Singlet oxygen, which also may be produced during photocatalysis, exhibits chemiluminescence at 1270 nm, which allows its facile fluorimetric determination [22].

4.2 Photocatalysis on Inorganic Semiconductors

Metal oxides were historically the first photocatalysts of the two-electron ORR discovered following the observation of light-induced degradation of organic matter in the presence of zinc and titanium white pigments. The photocatalytic activity of these pigments in ORR is due to a good match of their conducting band edge and the oxygen redox potentials (Fig. 4.2). Following this discovery, the photocatalytic activities of other transition metal oxides and related compounds were studied.

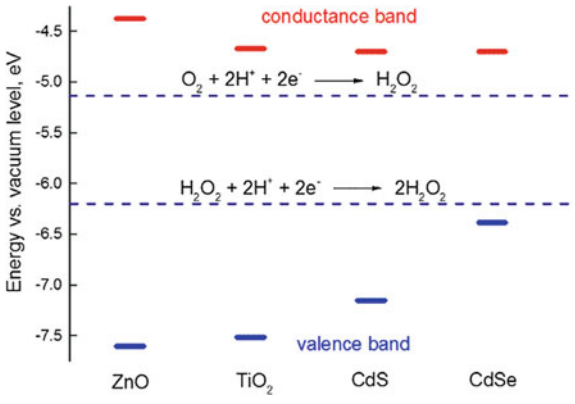

Fig. 4.2 Valence band and conductance band levels of ZnO, TiO_2, CdS and CdSe (data taken from [23]) and half reactions associated with ORR

4.2.1 Zinc Oxide

Zinc oxide is an *n*-type semiconductor with a band-gap of 3.37 eV [24], which effectively absorbs light up to 385 nm [25] (Fig. 4.3) and has a surface with high capacity of sorption of molecular oxygen [26]. The concentration of hydrogen peroxide achieved by photoreduction of molecular oxygen with pristine ZnO was shown to reach a plateau, with position determined by the form of the photocatalyst [27, 28], the nature and concentration of the oxidizable substance [29–34] and temperature. The highest level of H_2O_2 production comprising 0.06 mM or 9 μmol of H_2O_2 production per gram of pristine ZnO was observed in the absence of a sacrificial donor [35].

The mechanism of oxygen photoreduction by pristine ZnO was supposed to include the following steps: one-electron reduction of water at ZnO surface (4.7), addition of the resulting hydrogen radical to oxygen molecule (4.8), dismutation of the resulting superoxide to hydrogen peroxide and molecular oxygen (4.3), one-electron oxidation of the hydroxide anion at the surface of the photocatalyst to form a hydroxyl radical (4.9), and recombination of two hydroxyl radicals to form hydrogen peroxide (4.5) [11].

$$H_2O \xrightarrow{e} H^{\cdot} + OH^{-} \tag{4.7}$$

$$H^{\cdot} + O_2 \rightarrow HO_2^{\cdot} \tag{4.8}$$

$$OH^{-} \xrightarrow{h} OH^{\cdot} \tag{4.9}$$

$$ZnO + O_2 + 2H_2O \rightarrow H_2O_2 + Zn(OH)(OOH) \tag{4.10}$$

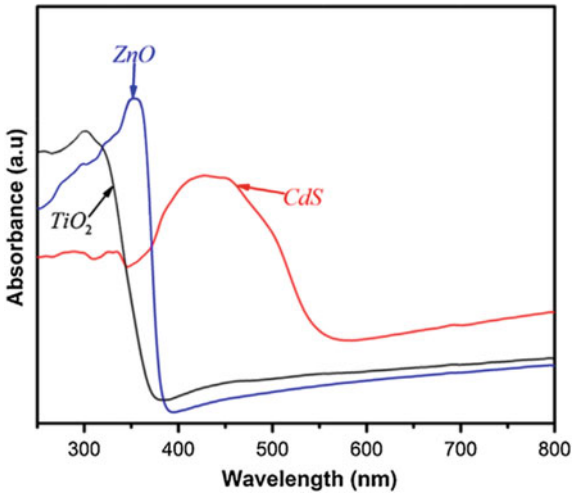

Fig. 4.3 Absorbance spectra of ZnO, TiO_2 and CdS. Image adapted from [36], Copyright 2015, with permission from Elsevier

The maximum quantum yield of the reaction, implying the formation of hydrogen peroxide in step (4.3) is 0.5. Hydroxyl recombination (4.5) which could give a quantum yield of up to 1, makes only a minor contribution to the formation of hydrogen peroxide, the majority of the peroxide particles remain bound to the surface in the form of zinc peroxyhydroxide, and eventually the material balance of the reaction is described by 4.10, which is confirmed by partial photodissolution of zinc oxide observed in the reaction [37]. Moreover, the adsorption of hydroxyl radicals passivates the catalyst surface and inhibits the formation of hydrogen peroxide.

Later studies using isotopically labeled oxygen, water, and zinc oxide [38], combined with the reaction kinetics studies [26, 39, 40] confirmed the one-electron oxygen reduction (4.3) to be the key step in the photocatalysis. An additional contribution to the formation of hydrogen peroxide is made by an electron transfer from the photocatalyst to hydrogen superoxide (4.11) [28], while additional ways of hydrogen peroxide decomposition are given by (4.12) and (4.13).

$$HO_2^{\cdot} + H^+ \xrightarrow{e} H_2O_2 \tag{4.11}$$

$$H_2O_2 + O_2^{\cdot -} \rightarrow OH^{\cdot} + OH^- + O_2 \tag{4.12}$$

$$H_2O_2 \xrightarrow{e} OH^{\cdot} + OH^- \tag{4.13}$$

The hydrogen peroxide formation obeys pseudo-zero order kinetics under continuous aeration, since it occurs under tremendous excess of the reactants (water, hydroxide ions and dissolved oxygen). The reactions consuming hydrogen peroxide have at least the first order kinetics in hydrogen peroxide. This creates the quasi-stationary conditions for the concentration of hydrogen peroxide, with the plateau concentration, $[H_2O_2]_{QS}$, depending only on the initial parameters of the system. In accord with this, addition of a surplus amount of H_2O_2 over $[H_2O_2]_{QS}$ leads to the restoration of a quasi-stationary value in the course of a photocatalytic reaction [11].

Sacrificial photocatalytic two-electron ORR on ZnO was reported for a wide set of reductants including formamide, acetamide, acetanilide and other amides [11], phenols [26, 29, 41], aliphatic alcohols [33, 35, 42, 43] and carboxylic acid salts [30, 38–40, 44]. The maximum H_2O_2 concentration achieved with pristine ZnO reaches 60 mM when isopropyl alcohol was used as a sacrificial donor [35].

In terms of the reaction mechanism, two principal schemes can be proposed for reactions with the addition of an oxidizable substrate. The first scheme implies the oxygen reduction (4.3) as anodic process and the oxidation of the sacrificial electron donor as cathodic process. Further transformations are individual for each substrate and can proceed both on the surface of the photocatalyst and in the solution. Most of the organic substrates are subsequently mineralized to CO_2, H_2O and N_2. The second scheme involves the oxidation of the substrate by hydroxyl radicals formed during the reduction of oxygen and the oxidation of water at the surface of the photocatalyst.

4.2.2 Titanium Dioxide

Titanium dioxide is an *i*-type semiconductor with a 3.24 eV band gap, which effectively absorbs light up to 400 nm [45] (Fig. 4.3). The advantages of titanium oxide as a photocatalyst are its high chemical and photochemical stability, as well as low dark catalytic activity with respect to the decomposition of hydrogen peroxide, unlike ZnO [46, 47].

The molecular mechanism of photocatalytic oxygen reduction on pristine TiO_2 is similar to that of ZnO. Molecular oxygen adsorbed on the catalyst surface is reduced at the catalyst surface upon photoexcitation of an electron from the valence band to the conduction band of TiO_2, the resulting superoxide particle then dismutates with the formation of hydrogen peroxide [48, 49]. In the absence of sacrificial donors, the holes in the valence band are quenched by the oxidation of hydroxide anions or water molecules to produce hydroxyl radicals.

The role of the electron donor is not limited to its function as a reductant. Some electron donors reduce the hydroxyl radicals formed in the above process, which prevents the surface passivation of the photocatalyst [48]. Others, known as redox mediators, such as formate ion, dimethylviologen dication or Cu^{2+} ions can facilitate electron transfer from the photocatalyst to the oxygen molecule, moving the process from the catalyst surface to the solution. The redox mediators may serve either as oxidation mediators for sacrificial donors, or as formate ion, as electron donors themselves [50].

Surface modification of TiO_2 is widely used to increase its photocatalytic activity in ORR by facilitating electron transfer, enhancing light absorption, increasing the catalyst stability or by suppressing the catalytic decomposition of hydrogen peroxide.

The success of these modifications requires careful optimization of the photocatalytic system. For example, fluorinated titania shows high $[H_2O_2]_{QS}$ in the presence of formate ions (7 mM), but with benzoate ions $[H_2O_2]_{QS}$ is much lower (0.035 mM) and exceeds that of pristine TiO_2 (0.07 mM) [50, 51]. Formate serves as a redox mediator, transporting an electron from the photocatalyst conduction band to dissolved oxygen, and acts as an effective hole suppressor for the valence band, inhibiting the oxidative photodecomposition of hydrogen peroxide. However, fluoride modification hinders the processes of electron transfer on the semiconductor surface for bulky electron donors, which is the reason for the decrease in performance observed in the case of benzoic acid [50].

The dopation of TiO_2 surface with Zn^{2+} inhibits the sorption of the radical and peroxide species, suppressing the unwanted side-processes [52]. More effective surface protection may be achieved with SnO_2 passivation coating [53].

A problem with the practical application of both TiO_2 and ZnO is their zero absorbance in the visible spectrum range. In case of TiO_2, this problem can be solved by dopation of the catalyst with nitrogen or sulfur atoms, which causes a redshift of ca. 100 nm of the absorbance edge [54]. When irradiated with blue light (λ_{max} 442 nm), both N- and S-doped catalyst exhibited non-sacrificial photocatalytic two-electron ORR activity and provided quasi-stationary peroxide concentration of

60 nM. An alternative way to enhance light absorbance is the surface modification with dyes, such as cobalt carboxylate [55] and phthalocyaninate [56]. The effect caused by the surface modification of titanium dioxide by Cu^{II} ions is more complex [57, 58]. On the one hand, due to the surface band gap narrowing, the material becomes active when irradiated with a wavelength of 450 nm. On the other hand, Cu^{2+} ions are reduced to Cu^{+} and Cu^{0} species, which serve as one- or two-electron redox mediators [58]. Titanium dioxide modified with copper ions is able to generate a quasi-stationary concentration of hydrogen peroxide 2.1 times greater than N-doped titanium dioxide under similar conditions. Surface modification of titanium dioxide by Rh^{III} ions causes a similar effect [59]. However, unlike copper ions, the main mechanism for the synthesis of hydrogen peroxide in this case is the two-electron reduction of oxygen by Rh^{I} particles. In addition, rhodium ions catalyze the oxidation of sacrificial electron donors on the surface of titanium dioxide. Direct two-electron ORR on TiO_2 can also be employed using 2-ethylanthraquinone as an "electron condenser" [60]. The name originates from the role of the anthraquinone compound, which undergoes two one-electron reductions followed by oxidation in a two-electron process. This approach allows hydrogen peroxide concentrations to reach up to 8.7 mM.

Nanoengineering of TiO_2-based photocatalysts leads to significant enhancement of its photocatalytic performance in ORR because the photocatalytic activity depends on the morphology of the photocatalyst particles [37, 45, 61]. Titanium dioxide exists in two modifications, anatase and rutile, with different photocatalytic activities. Anatase has been shown to produce greater quasi-stationary concentrations of hydrogen peroxide than rutile, and the mixed phase is superior in this respect to both modifications of pristine TiO_2 [62].

4.2.3 Other Inorganic Semiconductors

Other semiconductor oxides which demonstrate photocatalytic activity in two-electron ORR include Ga_2O_3, [41] Sb_2O_3 [63] and CuO [64]. Sb_2O_3 works in the UV-range (300 nm) and shows $[H_2O_2]_{QS}$ of 0.3 mM in non-sacrificial and 1 mM in sacrificial modes with glycerol as an electron donor [65]. CuO, due to the low band gap, absorbs light up to 660 nm, and exhibits a visible-light driven photocatalytic ORR. Unfortunately, due to the high catalytic activity of CuO for the decomposition of hydrogen peroxide, the achievable quasi-stationary concentration of H_2O_2 is relatively small [64]. The photocatalytic potential of Cu(II) is disclosed in combination with WO_3 as inert light harvesting matrix. When WO_3 is grafted with Cu^{2+} ions, which enable two-electron reduction of O_2, a high rate of H_2O_2 formation in the presence of acetaldehyde are observed upon illumination with 470 nm light. Low concentration of Cu^{2+} ions secures a negligible rate of H_2O_2 decomposition on WO_3/Cu^{2+} photocatalyst [57, 58].

In addition to metal oxides, a number of metal chalcogenides show photocatalytic activity in O_2 to H_2O_2 reduction. These compounds have often more narrow band

gap as compared to ZnO or TiO_2 and can operate in visual spectral range (e.g., see comparison of absorbance spectra for ZnO, TiO_2 and CdS in Fig. 4.3). For example, HgS shows catalytic activity at 600 nm providing up to 0.55 μM of H_2O_2 in a non-sacrificial mode [65]. Photocatalytic activity in a sacrificial mode at 365 nm with phenol as an electron donor has been tested for a wide set of chalcogenides, including ZnS, HgS, CdS, Ga_2S_3, CdSe, CdTe and ZnTe [41]. Within this series, CdS and CdSe exhibited the best performance, generating up to 1.7 and 1.0 mM of H_2O_2, respectively. Significant amounts of hydrogen peroxide above 0.3 mM were also detected in case of HgS and Ga_2S_3 [41].

4.2.4 *Inorganic Composite Photocatalysts*

The performance of the catalysts based on oxide or chalcogenide semiconductors relies on the construction of nanocomposites with a semiconductor-metal contact. Particles of noble metals such as platinum [66–69], gold [70–72] and binary Ag-Au alloys [73], when in contact with the oxide semiconductor, increase its photocatalytic activity and light efficiency. Photocatalysts of this type show quasi-stationary concentrations of hydrogen peroxide of up to 4.3 mM [68]. Particles of noble metals enhance the light efficiency due to plasmon resonance [74], catalyze one- and two-electron reductions of molecular oxygen [69] and increase the luminous efficiency and quantum yield of the charge separation process collecting the electrons from the semiconductor conduction band [71]. In some cases, nanoparticles of noble metal were shown to lead the oxygen reduction reaction exclusively to a two-electron reduction path [70] (Fig. 4.4). In addition, the modification of the semiconductor surface with noble metals prevents the accumulation of peroxide particles on the semiconductor surface due to inertness of the noble metal. This can also be the reason for the observed inhibition of the catalytic decomposition of H_2O_2 on catalyst particles by Ag-Au alloys [73]. Nanoensembles of TiO_2 with gold and platinum show enhanced

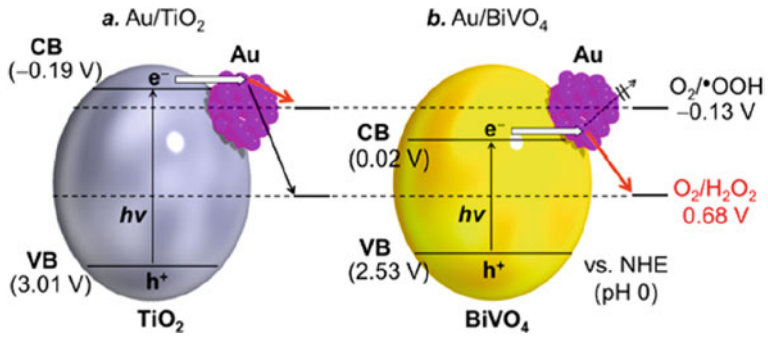

Fig. 4.4 Schematic representation of Au/TiO_2 and $Au/BiVO_4$ photocatalysts with energy diagram for photocatalysis. Adapted with permission from [70]. Copyright 2016 American Chemical Society

ORR photocatalytic performance, providing $[H_2O_2]_{QS}$ of 1.5 mM in a sacrificial mode [75, 76]. Only a subtle plasmonic resonance light utilization was observed in these cases, while the catalysis of charge transfer to O_2 is the main function of metal nanoparticles in such ensembles. The same effect is observed using polyoxymetallate covalent modification of TiO_2 surface [77]. ZnO photocatalyst may also be improved using the surface plasmon resonance of gold nanoparticles [74].

The second group of composite photocatalysts is a pair of semiconductors being in contact [78–86]. Such composites show an increase in luminous efficiency due to the electronic transitions now possible between the valence band of one semiconductor and the conduction band of another directly, or through the formation of an electron-hole pair in one semiconductor with the subsequent transition of an electron or hole to the other semiconductor. The main mechanism of such photocatalysis in most cases is photoelectrolysis, where the areas of electrode reactions are localized in different semiconductors.

The H_2O_2 formation rate on ZnO photocatalyst can be increased using this approach by dopation of ZnO with ruthenium oxide, which allows the harvesting of visible light up to 800 nm due to the narrow band gap between the conduction band of zinc oxide and the valence band of ruthenium oxide [87]. A similar effect is achieved with CdSe quantum dot sensitization [88]. Using $CoFe_2O_4$ spinel nanocrystals, double catalytic effect was achieved, improving both oxygen reduction and donor oxidation [89]. Recently, a great progress in the visible light harvesting of TiO_2 ORR photocatalysts was achieved by using nanostructured TiO_2 ensembles with quantum dots, which enhances the visible light absorption and facilitates charge separation due to Shottki effect [90]. Using highly structured TiO_2 particles, proton-form TiO_2 nanotubes modified with carbon quantum dots (Fig. 4.5), the millimolar concentrations of H_2O_2 may be achieved under 420 nm illumination [91]. WO_3-based heterojunction composites are also able to photocatalyze ORR. WO_3-melam particles exhibit high photocatalytic performance, producing up to 40 μM of H_2O_2 [92], as well as three-component composite particles, combining WO_3:TiO_2 heterojunction and WO_3:Pt surface modification.

Platinized Bi_2WO_6 [93], Bi_2O_3 surface-modified with Au nanoparticles [94] and mixed phase bismuth oxyhalides [95] also show the ORR photocatalytic performance with H_2O_2 concentrations up to 40 μM under 420–480 nm illumination. A sesame ball-like Ag_3PO_4@$CoFe_2O_4$ composite, irradiated with visible light, was found to produce up to 40 μM of H_2O_2 [96]. MoO_3/SnS_2 composite nanotubes deliver more than 120 μM of H_2O_2 under simulated sunlight [97]. The prominent photocatalytic ability was demonstrated by nanoporous-carbon supported Co_3O_4, which generates more than 1.5 mM of H_2O_2 under visible light [98]. An interesting example is composite particles, containing CdS spheres and graphene sheets modified with Pd^{II}-porphyrin and 9,10-ethynylphenylanthracene (Fig. 4.6), which provide up-conversion of photons in the red region of the spectrum and allow the use of light up to 650 nm, which increases the overall luminous efficiency of the system [83].

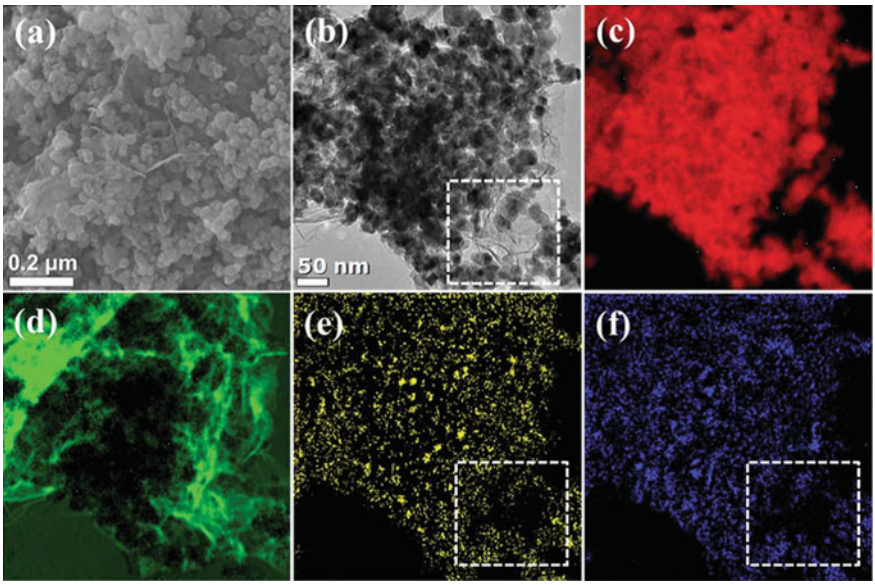

Fig. 4.5 **a** FE-SEM image and **b** TEM image of rGO/TiO_2 (including 6 wt% of rGO) after the irradiation for 3 h in the presence of cobalt and phosphate ions. **c–f** EELS mapping corresponding to panel (**b**). Red, green, yellow, and blue colour represent (**c**) titanium, (**d**) carbon, (**e**) phosphorus, and (**f**) cobalt element, respectively. Reprinted from [91], Copyright 2019, with permission from Elsevier

4.3 Carbon-Derived Photocatalysts

A broad spectrum of carbon-based materials and organic compounds demonstrates photocatalytic activity in two-electron oxygen reduction reaction. The solid state photocatalysts are presented by graphene oxide, carbon nitride and polyaromatic compounds. The molecular photocatalysts are presented mainly by anthracene, acridine and isoquinoline derivatives.

4.3.1 2D Carbon Materials

Graphene, the most simple in terms of molecular structure representative of 2D carbon materials, can enhance the photocatalytic performance of semiconductor solids similarly to nanoparticles of noble metals [99, 100]. Hybrid materials consisting of titanium oxide or cadmium sulfide in contact with graphene showed photocatalytic activity greater than the components of the materials taken separately.

Graphene oxide, which can be considered a surface O-modified graphene (Fig. 4.7), shows photocatalytic activity in two-electron oxygen reduction both as an individual component or in combination with semiconductor additives. The obtained

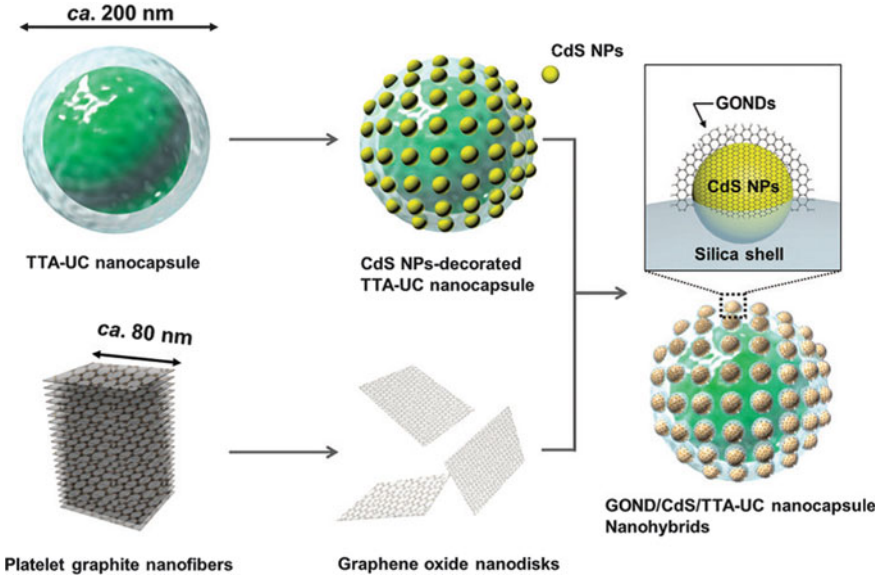

Fig. 4.6 Morphology of the composite up-conversion photocatalyst composed of CdS nanoparticles (NP) modified with graphene oxide nanodiscs (GOND). Republished with permission of The Royal Society of Chemistry from [83] Copyright 2016, permission conveyed through Copyright Clearance Center, Inc.

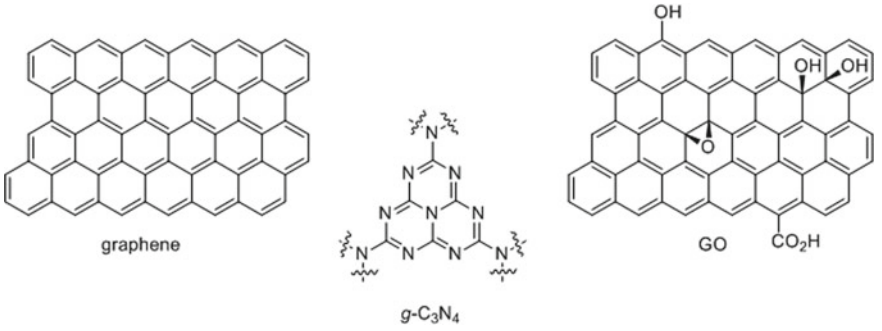

Fig. 4.7 2D carbon materials: graphene, graphene oxide (GO) and graphitic carbon nitride (g-C_3N_4)

maximum quasi-stationary concentrations of H_2O_2 comprised 1.5 mM in pure water, which could be increased to 4 mM when sacrificial reductants were used [101]. Further increase was achieved by modification of graphene oxide with cadmium polynuclear complexes, which afforded up to 7 mM of H_2O_2 under visible light irradiation [102].

Heteroatom-doped graphene quantum dots showed more modest performance as oxygen reduction catalysts, yielding up to 0.5 mM H_2O_2 concentrations [103].

The best performance within the family of carbon materials show graphitic carbon nitride photocatalysts extensively studied during the past few years [9, 104–107]. The g-C_3N_4 nanostructures (Fig. 4.7), modified with different inorganic and/or organic compounds, are able to produce millimolar quantities of H_2O_2 utilizing nearly the whole visible spectrum [108].

4.3.2 Polyaromatic Compounds

In addition to the classical inorganic semiconductors, organic and organometallic semiconductors are used for photocatalytic oxygen reduction. An important advantage of these catalysts is the possibility of fine tuning of their properties by modifying an organic molecule.

A series of p-type semiconductor cobalt, iron and zinc porphyrinates and phthalocyaninates **1**–**5** (Fig. 4.8) adsorbed on Nafion membranes was tested [109]. Irradiation of such membranes with visible light in the presence of triethylammonium perchlorate in the system leads to the formation of micromolar quasi-stationary concentrations of hydrogen peroxide on a μM scale. Better results demonstrated polythiophene with 0.1 mM H_2O_2 concentration in a non-sacrificial photocatalitic ORR.

An improved ORR photocatalytic behavior of n-type organic semiconductors was demonstrated using acene-based biscoumarins **6**-**8** (Fig. 4.8), which show the non-sacrificial H_2O_2 production under visible light with a rate up to 3.3 mg per 1 g of catalyst per 1 h [110]. Nearly the same non-sacrificial photocatalytic performance was observed using the resorcinol-formaldehyde resins as n-type semiconductors,

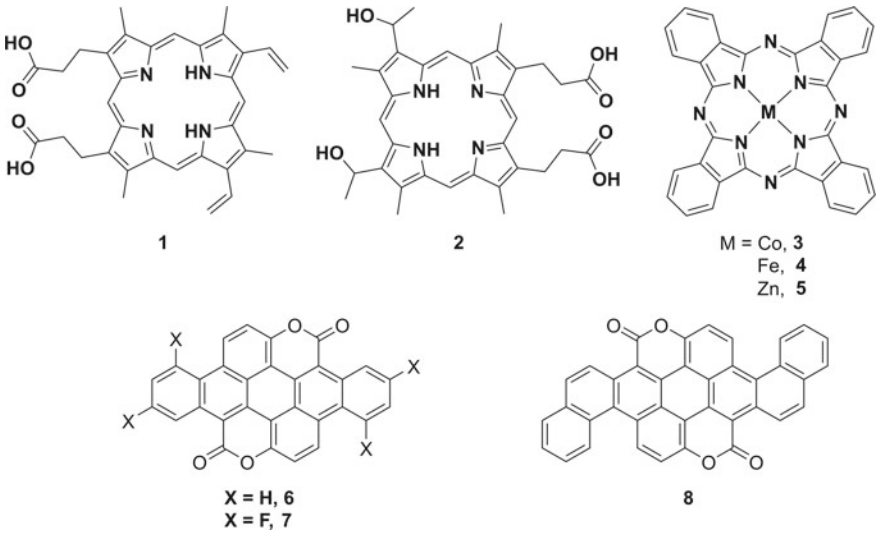

Fig. 4.8 Structure of organic semiconductors **1-8**

harvesting light up to 700 nm and producing more than 60 μM of hydrogen peroxide in water [111]. Another n-type semiconductor, perylene diimide, produced up to 3 mM hydrogen peroxide concentration with oxalate as a sacrificial electron donor [112]. Acetylene-extended triazine covalent frameworks afford up to 70 μM of H_2O_2 under the same operation conditions [113].

The semiconductive microcrystals of coordination polymer derived from Cd^{2+} and thiocyanuric acid is an interesting example of a metal complex semiconductor photocatalyst [114]. The maximum concentration of hydrogen peroxide achieved with the addition of methanol was 8.75 mM. The authors suggest a single-electron oxygen reduction mechanism.

4.3.3 Metal Complexes with Organic Ligands as Homogeneous Photocatalysts

Ru^{II} complexes with *N*,*N*-bidentate ligands based on bipyridyl fragment, like compounds **9** and **10** (Fig. 4.9) are well studied ORR photocatalysts with good performance [115–120]. For example, compound **9** was found to produce a hydrogen peroxide with concentration of 0.57 mM upon visible light illumination in the presence of ascorbic acid [116].

High chemical and photolytic stability, combined with a sufficiently long lifetime of the triplet excited state (600 ns) and absorption in the visible region of the spectrum ($\lambda_{max} \sim 450$ nm) make them convenient photocatalysts [121]. Kinetic studies revealed the one-electron oxygen reduction (4.2) to be the key step of Ru-photocatalyzed ORR [115]. Depending on the sacrificial donor, either dismutation (4.3) or the reduction of superoxide by sacrificial donor leads then to the formation of H_2O_2.

In order to increase the electron transfer rate from the photocatalyst to molecular oxygen, various redox mediators are widely used. The maximum concentration of hydrogen peroxide achieved using **9** as a photocatalyst and dimethyl viologen as redox mediator for one-electron oxygen reduction with the addition of formic acid was about 0.35 mM [118].

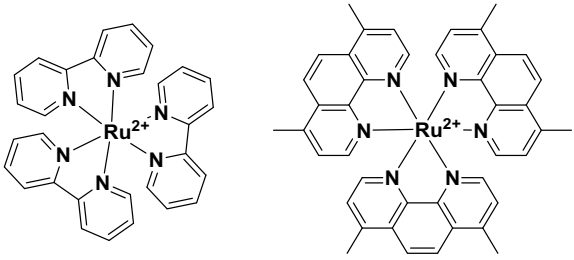

9 10

Fig. 4.9 Structures of Ru^{II} photocatalysts

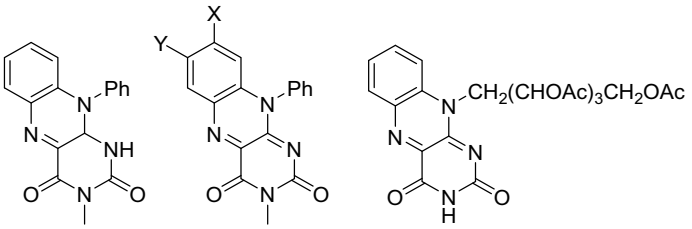

11 X = Y = H, **12**
X = Cl, Y = H, **13**
X = H, Y = NO_2, **14**
15

Fig. 4.10 Flavins **11-15**

An alternative way to enhance electron transfer is to stabilize the resulting product of one-electron O_2 reduction, the superoxide anion. Hence, ions of rare earth metals such as Sc^{3+}, Y^{3+}, Yb^{3+}, Lu^{3+} were found to co-catalyze photocatalytic ORR with ruthenium complexes by coordinating the reaction product, superoxide anion [122–125].

For non-sacrificial photocatalytic ORR, water oxidation usually represents a bottleneck of the process, which may be overcome using water oxidation catalysts. Polynuclear complex $Fe_3[Co(CN)_6]_2$ [122–124] as well as inorganic semiconductors $Ir(OH)_3$, WO_3 and $BiVO_4$ [122, 125] can enhance the Ru^{II} catalyzed ORR by mediating water oxidation. This approach allows to obtain a 0.4 mM quasi-stationary concentration of hydrogen peroxide without any oxidizable additives.

A combination of these approaches in a multicomponent system for nonsacrificial photocatalytical ORR, consisting of ruthenium-based ORR catalyst with Sc^{3+} as a co-catalyst and $NiFe_2O_4$ nanoparticle for simultaneous water oxidation, was reported to produce up to 1.4 mM H_2O_2 concentration [126].

Due to the high cost of ruthenium, cheaper alternatives are actively sought. An example can be zinc and magnesium complexes of flavins **11-14** (Fig. 4.10) or scandium and lanthanoide 2:1 complexes with flavin **15**, which also demonstrate photocatalytic activity in ORR. Under illumination with visible light, the complex of **11** with Mg^{2+} produces up to 2 mM concentration of H_2O_2 with benzylic alcohol as a sacrificial electron donor [127]. Within this series, the highest quasi-stationary concentration of hydrogen peroxide of 2.8 mM was achieved with **15**-Lu^{3+} as a photocatalyst and 4-methoxybenzyl alcohol as an oxidizable additive [128].

4.3.4 Anthraquinone Derivatives

The ability of anthraquinone to photochemically oxidize organic matter, combined with the well-known two-electron reduction of molecular oxygen by 2H-anthraquinone, inspired the application of anthraquinone derivatives in photocatalytical ORR.

In the presence of a sacrificial hydrogen donor like ethanol, anthraquinone was reported to be photoreduced to 2H-anthraquinone, which then reduces dioxygen in a two-electron reduction step similar to the dark process (Fig. 4.11). For example, a quasi-stationary concentration of hydrogen peroxide of ca. 360 mM was achieved with 2-ethylanthraquinone at exposure to simulated sunlight [129].

When no convenient hydrogen source is present, the photocatalytic process was described to proceed as one-electron oxidation of sacrificial donor followed by one-electron reduction of dioxygen (Fig. 4.11). In both cases the active form is the long-living triplet state of anthraquinone catalyst (ca. 10 μs), which either abstracts hydrogen atom from a hydrogen donor or mediates electron transfer from the reductant to dioxygen via radical anion species [130].

For practical applications, two-phase water/organic solvent systems are convenient, like water/ethyl acetate, water/toluene, water/xylene and water/mesitylene. In these systems, hydrogen peroxide formed during the reaction in the organic phase is extracted into the aqueous phase. The highest H_2O_2 concentration of 0.5 M was achieved within this series for water/mesitylene system [129].

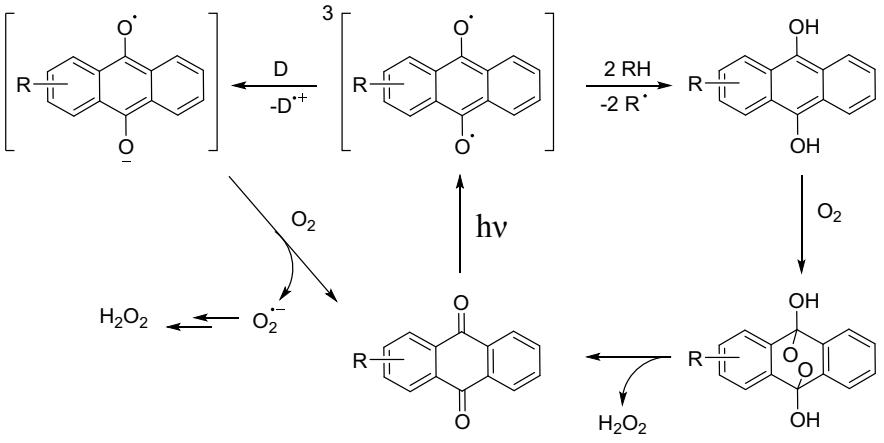

Fig. 4.11 Scheme of the photocatalytic production of hydrogen peroxide using anthraquinones

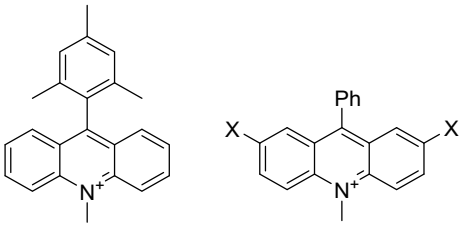

Fig. 4.12 Structures of the acridinium photocatalysts

4.3.5 Acridinium Photocatalysts

9-Aryl-10-methylacridinium derivatives (Fig. 4.12) are an interesting class of homogeneous photocatalysts, due to the long lifetime and high energy of the charge shifted state (2.37 eV for **16**) formed upon photoexcitation of these molecules [131].

The formation of hydrogen peroxide was observed as an oxygen reduction product with a yield close to quantitative in the process of photocatalytic oxidation of anthracene to anthraquinone with atmospheric oxygen catalyzed by **16** in acetonitrile upon irradiation at 430 nm [132]. The extract of coal tar, which consists mostly of anthracene, was proposed as a cheap oxidizable additive for the synthesis of hydrogen peroxide [133]. Irradiation of an aerated solution of coal tar extract and photocatalyst **16** in acetonitrile with light at 430 nm resulted in the formation of a 0.47 mM hydrogen peroxide solution. In these reactions, oxidation of the anthracene with charge separated state of **16** is the first step, followed by the electron transfer from the reduced photocatalyst to an oxygen molecule. The electron transfer from the semi-oxidized intermediate of anthracene, 10-hydroxyanthrone, leads to reduction of the superoxide to yield the hydrogen peroxide molecule, efficiently suppressing its dismutation. The formation of the hydrogen peroxide was also detected in photocatalytic oxidation of cyclohexane [134] and Fe^{II} [135] complexes with **16**.

Similar photocatalytic oxidation of methylbenzenes and benzylic alcohols to corresponding benzaldehydes with catalysts **16-18** leads to the formation of hydrogen peroxide, although the non-polarized singlet excited state is responsible for the process in case of **17** and **18** [136, 137].

The formation of the hydrogen peroxide was also detected in photocatalytic oxidation of cyclohexane and Fe^{II} complexes with **16** [134, 135].

4.3.6 Quinolinium Photocatalysts

Quinolinium (**19**-**22**) and isoquinolinium (**23**) compounds (Fig. 4.13) demonstrate both types of photoredox activity, through strongly oxidizing electronically excited singlet state and through charge-separated state.

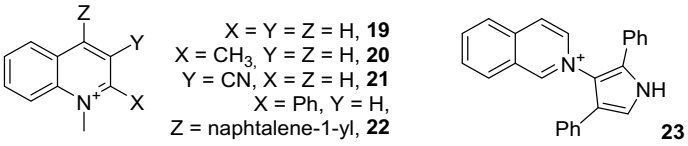

Fig. 4.13 Structures of (iso)quinolinium ORR photocatalysts

An example of the first type, compound **21**, has the first singlet excited state with oxidative potential of 2.72 V. This allows simultaneous H_2O_2 production and selective oxidative transformations of a wide range of organic sacrificial donors [138].

The photocatalytic activity of compound **21** in the acetonitrile-water-benzene system was investigated upon irradiation with light with a wavelength of 290–400 nm [138]. During the reaction, the $[H_2O_2]_{QS}$ of 15 mM was achieved, with phenol being the main oxidation product in 41% yield, 98% selectivity and 16% quantum yield. Catalysts **19**-**20** exhibit similar activity, but give lower yield and selectivity. The use of chlorobenzene instead of benzene as an oxidizable additive leads to the formation of a mixture of 4-chlorophenol and 2-chlorophenol in 27% and 3% yields with a selectivity of 31%. Along with hydrogen peroxide formation, an alkoxylation of arenes takes place, when an alcohol is used as a nucleophile instead of water [139]. Similarly, using fluoride ion as a nucleophile, fluorination of benzene can be achieved along with the formation of hydrogen peroxide [140]. The maximum concentration of hydrogen peroxide in this photocatalytic system reaches 8 mM. The reaction mechanism of ORR photocatalyzed by **21** in the presence of benzene includes preliminary one-electron oxidation of arene by the singlet excited state of **21** with subsequent one-electron transfer from the reduced catalyst to oxygen molecule. Nucleophilic addition to the resulting benzene radical-cation occurs, followed by radical quenching with oxygen molecule [138–140].

Compound **22** (Fig. 4.13) is an example of the second type of photocatalytic activity, which proceeds through the formation of the charge separated state. This molecule, due to the combination of donor and acceptor fragments, forms a charge transfer state with a lifetime of 500 fs upon photoexcitation [141]. In the photoredox catalytic cycle of oxygen reduction by oxalate ions in aqueous acetonitrile, the electronically excited **22** reduces the oxygen molecule and then the resulting dication-radical oxidizes the oxalate ion. Overall, the yield of peroxide on oxalate reaches 93% and the quantum yield is 14%. The oxalate is a prospective sacrificial electron donor as it is a by-product in wood industry and because it gives carbon dioxide as the only oxidation product.

Photocatalytic oxygen reduction by oxalate ions is sensitive to *p*H of the medium. A great enhancement of the H_2O_2 production was found with the addition of acetate ions, and the maximum concentration of hydrogen peroxide of 70 mM was reached in this case. The acetate ion was suggested to play the role of a proton transporter in acetonitrile, facilitating deprotonation of oxalic acid and protonation of a superoxide ion [142].

Compound **22** can be used also in water but in a heterogenous mode, when sorbed into a mesoporous silica-alumina sorbent [143]. The resulting composite catalyst gives a quasi-stationary concentration of hydrogen peroxide of 4 mM and a quantum yield of 10%.

Homogeneous photocatalytic ORR in aqueous solution was achieved with pyrrolo-isoquinolinium dyad **23** [144]. With this photocatalyst in an oxalate-containing aqueous solution illuminated with 420 nm light, a concentration of H_2O_2 exceeds 1 mM. The oxidation of the oxalate with the excited state of **20** was found to be the first step of the process, followed by the electron transfer to the oxygen molecule. Most probably, the active intermediate is the charge-separated state of **23**.

4.4 Conclusions

Starting from the middle of twentieth century, a wide range of classes of inorganic and organic materials were found to exhibit photocatalytic reduction of molecular oxygen to hydrogen peroxide. To improve photocatalytic ORR performance of semiconductor photocatalysts, several pathways have been formulated. To increase the luminous efficiency of the photocatalysts, the optical band gap may be narrowed by heterojunction with another semiconductors or quantum dots, or by introduction of ions or molecules which have discreet energy levels within the band gap of the semiconductor. Modification of semiconductor surface with noble metal particles enables an extensive visible light utilization via the surface plasmon resonance, while modification of semiconductor particles with dyes leads to its sensibilisation. ORR kinetics may be facilitated using surface-bound or dissolved redox mediators, for example, transition metal ions, or switched from unfavorable one-electron oxygen reduction to the two-electron process using “electron condensers”.

Alternative to inorganic semiconductors, carbon-based materials or organic compounds can be employed as photocatalysts for conversion of oxygen to hydrogen peroxide. These compounds bear fused aromatic or electron-poor heteroaromatic rings as a key structural motif. The mechanism of photocatalytic oxygen reduction using these compounds proceeds through an energy-rich electronically excited state of the catalyst, which can be of triplet or highly polarized singlet character.

References

1. R.S. Disselkamp, Energy Fuels **22**, 2771 (2008)
2. G. Goor, J. Glenneberg, S. Jacobi, J. Dadabhoy, E. Candido, *Ullmann’s Encyclopedia of Industrial Chemistry* (Wiley-VCH Verlag GmbH & Co. KGaA, 2019)
3. E. Baur, C. Neuweiler, Helv. Chim. Acta **10**, 901 (1927)
4. A.H. Mehler, Arch. Biochem. Biophys. **33**, 65 (1951)
5. S. Fukuzumi, Biochim. Biophys. Acta **1857**, 604 (2016)
6. S. Fukuzumi, Y.M. Lee, W. Nam, Chemistry **24**, 5016 (2018)

7. J. Highfield, Molecules **20**, 6739 (2015)
8. C. Wang, X. Zhang, Y. Liu, Appl. Surf. Sci. **358**, 28 (2015)
9. Z. Haider, H.-I. Cho, G.-H. Moon, H.-I. Kim, Catal. Today **335**, 55 (2019)
10. S.G. Bratsch, J. Phys. Chem. Ref. Data **18**, 1 (1989)
11. M.C. Markham, K.J. Laidler, J. Phys. Chem. **57**, 363 (1953)
12. S.B. Brown, P. Jones, A. Suggett, Anal. Chim. Acta **43**, 343 (1968)
13. T.C.J. Ovenston, W.T. Rees, Analyst **75**, 204 (1950)
14. W. Masschelein, M. Denis, R. Ledent, Water Sewage Works **124**, 69 (1977)
15. R.M. Sellers, Analyst **105**, 950 (1980)
16. M. Zhu, X. Huang, L. Liu, H. Shen, Talanta **44**, 1407 (1997)
17. A.N. Díaz, F.G. Sanchez, J.A.G. García, Anal. Chim. Acta **327**, 161 (1996)
18. W. Chen, S. Cai, Q.Q. Ren, W. Wen, Y.D. Zhao, Analyst **137**, 49 (2012)
19. A. Takahashi, K. Hashimoto, S. Kumazawa, T. Nakayama, Anal. Sci. **15**, 481 (1999)
20. S.M. Steinberg, Environ. Monit. Assess. **185**, 3749 (2013)
21. H.C. Hu, H.J. Jin, X.S. Chai, J. Chromatogr. A **1235**, 182 (2012)
22. S. Zhao, X. Zhao, Appl. Catal. B **250**, 408 (2019)
23. V. Stevanovic, S. Lany, D.S. Ginley, W. Tumas, A. Zunger, Phys. Chem. Chem. Phys. **16**, 3706 (2014)
24. J. Anderson, G.V.d.W. Chris, Rep. Prog. Phys. **72**, 126501 (2009)
25. C.F. Goodeve, Trans. Faraday Soc. **33**, 340 (1937)
26. X. Domènech, J.A. Ayllón, J. Peral, Environ. Sci. Pollut. Res. **8**, 285 (2001)
27. G. Winter, Nature **163**, 326 (1949)
28. Y. Liu, J. Han, W. Qiu, W. Gao, Appl. Surf. Sci. **263**, 389 (2012)
29. M.C. Markham, M.C. Hannan, S.W. Evans, J. Am. Chem. Soc. **76**, 820 (1954)
30. C.B. Vail, J.P. Holmquist, L. White, J. Am. Chem. Soc. **76**, 624 (1954)
31. J.C. Young, E.P. Guth, J. Am. Pharm. Assoc. **45**, 724 (1956)
32. M.C. Markham, J.C. Kuriacose, J. DeMarco, C. Giaquinto, J. Phys. Chem. **66**, 932 (1962)
33. C. Kormann, D.W. Bahnemann, M.R. Hoffmann, Environ. Sci. Technol. **22**, 798 (1988)
34. E.R. Carraway, A.J. Hoffman, M.R. Hoffmann, Environ. Sci. Technol. **28**, 786 (1994)
35. J.C. Kuriacose, M.C. Markham, J. Catal. **1**, 498 (1962)
36. M.A. Gondal, A.M. Ilyas, T.A. Fasasi, M.A. Dastageer, Z.S. Seddigi, T.F. Qahtan, M. Faiz, G.D. Khattak, Appl. Surf. Sci. **357**, 2217–2222 (2015)
37. B. Pal, M. Sharon, Toxicol. Environ. Chem. **78**, 233 (2000)
38. J.G. Calvert, K. Theurer, G.T. Rankin, W.M. MacNevin, J. Am. Chem. Soc. **76**, 2575 (1954)
39. D. Dixon, T. Healy, Aust. J. Chem. **24**, 1193 (1971)
40. J.R. Harbour, M.L. Hair, J. Phys. Chem. **83**, 652 (1979)
41. R.E. Stephens, B. Ke, D. Trivich, J. Phys. Chem. **59**, 966 (1955)
42. M.C. Markham, M.C. Upreti, J. Catal. **4**, 229 (1965)
43. G. Irick, J. Appl. Polym. Sci. **16**, 2387 (1972)
44. T.R. Rubin, J.G. Calvert, G.T. Rankin, W. MacNevin, J. Am. Chem. Soc. **75**, 2850 (1953)
45. A.L. Linsebigler, G. Lu, J.T. Yates, Chem. Rev. **95**, 735 (1995)
46. C.M. Lousada, A.J. Johansson, T. Brinck, M. Jonsson, J. Phys. Chem. C **116**, 9533 (2012)
47. B. Jenny, P. Pichat, Langmuir **7**, 947 (1991)
48. V. Diesen, M. Jonsson, J. Phys. Chem. C **118**, 10083 (2014)
49. T. Hirakawa, H. Kominami, B. Ohtani, Y. Nosaka, J. Phys. Chem. B **105**, 6993 (2001)
50. M. Mrowetz, E. Selli, New J. Chem. **30**, 108 (2006)
51. V. Maurino, C. Minero, G. Mariella, E. Pelizzetti, Chem. Commun. **20**, 2627 (2005)
52. V. Maurino, C. Minero, E. Pelizzetti, G. Mariella, A. Arbezzano, F. Rubertelli, Res. Chem. Intermed. **33**, 319 (2007)
53. G. Zuo, B. Li, Z. Guo, L. Wang, F. Yang, W. Hou, S. Zhang, P. Zong, S. Liu, X. Meng, Y. Du, T. Wang, V.A.L. Roy, Catalysts **9**, 623 (2019)
54. T. Hirakawa, Y. Nosaka, J. Phys. Chem. C **112**, 15818 (2008)
55. T. Baran, S. Wojtyła, A. Minguzzi, S. Rondinini, A. Vertova, Appl. Catal. B **244**, 303 (2019)
56. A.P. Hong, D.W. Bahnemann, M.R. Hoffmann, J. Phys. Chem. **91**, 2109 (1987)

57. H. Irie, S. Miura, K. Kamiya, K. Hashimoto, Chem. Phys. Lett. **457**, 202 (2008)
58. Y. Nosaka, S. Takahashi, H. Sakamoto, A.Y. Nosaka, J. Phys. Chem. C **115**, 21283 (2011)
59. S. Kitano, N. Murakami, T. Ohno, Y. Mitani, Y. Nosaka, H. Asakura, K. Teramura, T. Tanaka, H. Tada, K. Hashimoto, H. Kominami, J. Phys. Chem. C **117**, 11008 (2013)
60. D. Zhang, G. Xu, T. Chen, F. Chen, RSC Adv. **4**, 52199 (2014)
61. F. Shiraishi, C. Kawanishi, J. Phys. Chem. A **108**, 10491 (2004)
62. H. Goto, Y. Hanada, T. Ohno, M. Matsumura, J. Catal. **225**, 223 (2004)
63. M.C. Markham, M.C. Hannan, L. Lin, C. Coffey, B. Jones, J. Phys. Chem. **62**, 989 (1958)
64. J. Bandara, I. Guasaquillo, P. Bowen, L. Soare, W.F. Jardim, J. Kiwi, Langmuir **21**, 8554 (2005)
65. L.I. Grossweiner, J. Phys. Chem. **59**, 742 (1955)
66. W. Zhao, C. Chen, X. Li, J. Zhao, H. Hidaka, N. Serpone, J. Phys. Chem. B **106**, 5022 (2002)
67. F. Shiraishi, T. Nakasako, Z. Hua, J. Phys. Chem. A **107**, 11072 (2003)
68. M. Teranishi, S.-I. Naya, H. Tada, J. Am. Chem. Soc. **132**, 7850 (2010)
69. V.M. Daskalaki, P. Panagiotopoulou, D.I. Kondarides, Chem. Eng. J. **170**, 433 (2011)
70. H. Hirakawa, S. Shiota, Y. Shiraishi, H. Sakamoto, S. Ichikawa, T. Hirai, ACS Catal. **6**, 4976 (2016)
71. M. Teranishi, R. Hoshino, S.-I. Naya, H. Tada, Angew. Chem. Int. Ed. **55**, 12773 (2016)
72. M. Teranishi, S.-I. Naya, H. Tada, J. Phys. Chem. C **120**, 1083 (2016)
73. D. Tsukamoto, A. Shiro, Y. Shiraishi, Y. Sugano, S. Ichikawa, S. Tanaka, T. Hirai, ACS Catal. **2**, 599 (2012)
74. X. Meng, P. Zong, L. Wang, F. Yang, W. Hou, S. Zhang, B. Li, Z. Guo, S. Liu, G. Zuo, Y. Du, T. Wang, V.A.L. Roy, Catal. Commun. **134**, 105860 (2020)
75. M.V. Dozzi, L. Prati, P. Canton, E. Selli, Phys. Chem. Chem. Phys. **11**, 7171 (2009)
76. K. Kim, J. Park, H. Kim, G.Y. Jung, M.-G. Kim, ACS Catal. **9**, 9206 (2019)
77. X. Wu, X. Zhang, S. Zhao, Y. Gong, R. Djellabi, S. Lin, X. Zhao, Appl. Catal. A **591**, 117271 (2020)
78. H. Chen, W. Leng, Y. Xu, J. Phys. Chem. C **118**, 9982 (2014)
79. C. Wang, X. Zhang, B. Yuan, Y. Wang, P. Sun, D. Wang, Y. Wei, Y. Liu, Chem. Eng. J. **237**, 29 (2014)
80. X. Zong, H. Chen, B. Seger, T. Pedersen, M.S. Dargusch, E.W. McFarland, C. Li, L. Wang, Energy Environ. Sci. **7**, 3347 (2014)
81. K. Fuku, K. Sayama, Chem. Commun. **52**, 5406 (2016)
82. M. Jakešová, D.H. Apaydin, M. Sytnyk, K. Oppelt, W. Heiss, N.S. Sariciftci, E.D. Głowacki, Adv. Funct. Mater. **26**, 5248 (2016)
83. H.-I. Kim, O.S. Kwon, S. Kim, W. Choi, J.-H. Kim, Energy Environ. Sci. **9**, 1063 (2016)
84. K. Mase, M. Yoneda, Y. Yamada, S. Fukuzumi, ACS Energy Lett. **1**, 913 (2016)
85. O. Tomita, T. Otsubo, M. Higashi, B. Ohtani, R. Abe, ACS Catal. **6**, 1134 (2016)
86. T. Fukumura, S. Akane, E. Sambandan, React. Kinet. Mech. Catal. **121**, 785 (2017)
87. J.Z. Bloh, R. Dillert, D.W. Bahnemann, Phys. Chem. Chem. Phys. **16**, 5833 (2014)
88. F. Donat, S. Corbel, H. Alem, S. Pontvianne, L. Balan, G. Medjahdi, R. Schneider, Beilstein J. Nanotechnol. **8**, 1080 (2017)
89. M. Chen, Y. Xu, Langmuir **35**, 9334 (2019)
90. P. Wang, D. Li, J. Chen, X. Zhang, J. Xian, X. Yang, X. Zheng, X. Li, Y. Shao, Appl. Catal. B **160–161**, 217 (2014)
91. R. Ma, L. Wang, H. Wang, Z. Liu, M. Xing, L. Zhu, X. Meng, F.-S. Xiao, Appl. Catal. B **244**, 594 (2019)
92. Z. Jin, Q. Zhang, L. Hu, J. Chen, X. Cheng, Y.-J. Zeng, S. Ruan, T. Ohno, Appl. Catal. B **205**, 569 (2017)
93. J. Sheng, X. Li, Y. Xu, ACS Catal. **4**, 732 (2014)
94. H.Y. Jiang, K. Cheng, J. Lin, Phys. Chem. Chem. Phys. **14**, 12114 (2012)
95. G. Liu, T. Wang, S. Ouyang, L. Liu, H. Jiang, Q. Yu, T. Kako, J. Ye, J. Mater. Chem. A **3**, 8123 (2015)

96. S. Huang, Y. Xu, Q. Liu, T. Zhou, Y. Zhao, L. Jing, H. Xu, H. Li, Appl. Catal. B **218**, 174 (2017)
97. Y. Zhang, S.-J. Park, J. Mater. Chem. A **6**, 20304 (2018)
98. C. Zhu, M. Zhu, Y. Sun, Y. Zhou, J. Gao, H. Huang, Y. Liu, Z. Kang, ACS Appl. Energy Mater. **2**, 8737 (2019)
99. G.-H. Moon, W. Kim, A.D. Bokare, N.-E. Sung, W. Choi, Energy Environ. Sci. **7**, 4023 (2014)
100. S. Thakur, T. Kshetri, N.H. Kim, J.H. Lee, J. Catal. **345**, 78 (2017)
101. W.-C. Hou, Y.-S. Wang, ACS Sustain. Chem. Eng. **5**, 2994 (2017)
102. J. Xu, Z. Chen, H. Zhang, G. Lin, H. Lin, X. Wang, J. Long, Sci. Bull. **62**, 610 (2017)
103. L. Zheng, H. Su, J. Zhang, L.S. Walekar, H. Vafaei Molamahmood, B. Zhou, M. Long, Y.H. Hu, Appl. Catal. B **239**, 475 (2018)
104. Y. Shiraishi, S. Kanazawa, Y. Sugano, D. Tsukamoto, H. Sakamoto, S. Ichikawa, T. Hirai, ACS Catal. **4**, 774 (2014)
105. Y. Shiraishi, Y. Kofuji, H. Sakamoto, S. Tanaka, S. Ichikawa, T. Hirai, ACS Catal. **5**, 3058 (2015)
106. Y. Kofuji, S. Ohkita, Y. Shiraishi, H. Sakamoto, S. Tanaka, S. Ichikawa, T. Hirai, ACS Catal. **6**, 7021 (2016)
107. S. Li, G. Dong, R. Hailili, L. Yang, Y. Li, F. Wang, Y. Zeng, C. Wang, Appl. Catal. B **190**, 26 (2016)
108. L. Zhou, J. Feng, B. Qiu, Y. Zhou, J. Lei, M. Xing, L. Wang, Y. Zhou, Y. Liu, J. Zhang, Appl. Catal. B **267** (2020)
109. J. Premkumar, R. Ramaraj, J. Mol. Catal. A: Chem. **142**, 153 (1999)
110. M.K. Węcławski, M. Jakešová, M. Charyton, N. Demitri, B. Koszarna, K. Oppelt, S. Sariciftci, D.T. Gryko, E.D. Głowacki, J. Mater. Chem. A **5**, 20780 (2017)
111. Y. Shiraishi, T. Takii, T. Hagi, S. Mori, Y. Kofuji, Y. Kitagawa, S. Tanaka, S. Ichikawa, T. Hirai, Nat. Mater. **18**, 985 (2019)
112. M. Gryszel, M. Sytnyk, M. Jakesova, G. Romanazzi, R. Gabrielsson, W. Heiss, E.D. Glowacki, ACS Appl. Mater. Interfaces **10**, 13253 (2018)
113. L. Chen, L. Wang, Y. Wan, Y. Zhang, Z. Qi, X. Wu, H. Xu, Adv. Mater. **32**, e1904433 (2020)
114. H. Zhuang, L. Yang, J. Xu, F. Li, Z. Zhang, H. Lin, J. Long, X. Wang, Sci. Rep. **5**, 16947 (2015)
115. Y. Kurimura, R. Onimura, Inorg. Chem. **19**, 3516 (1980)
116. K. Yoshimi, Y. Hiroshi, M. Yuko, Bull. Chem. Soc. Jpn. **54**, 2450 (1981)
117. Y. Kurimura, M. Nagashima, K. Takato, E. Tsuchida, M. Kaneko, A. Yamada, J. Phys. Chem. **86**, 2432 (1982)
118. M. Fukushima, K. Tatsumi, S. Tanaka, H. Nakamura, Environ. Sci. Technol. **32**, 3948 (1998)
119. A. Das, V. Joshi, D. Kotkar, V.S. Pathak, V. Swayambunathan, P.V. Kamat, P.K. Ghosh, J. Phys. Chem. A **105**, 6945 (2001)
120. J. Premkumar, R. Ramaraj, J. Chem. Soc. Dalton Trans., 3667 (1998)
121. C.-T. Lin, N. Sutin, J. Phys. Chem. **80**, 97 (1976)
122. S. Kato, J. Jung, T. Suenobu, S. Fukuzumi, Energy Environ. Sci. **6**, 3756 (2013)
123. Y. Isaka, K. Oyama, Y. Yamada, T. Suenobu, S. Fukuzumi, Catal. Sci. Technol. **6**, 681 (2016)
124. J.W. Han, J. Jung, Y.-M. Lee, W. Nam, S. Fukuzumi, Chem. Sci. **8**, 7119 (2017)
125. Y. Isaka, Y. Yamada, T. Suenobu, T. Nakagawa, S. Fukuzumi, RSC Adv. **6**, 42041 (2016)
126. Y. Isaka, S. Kato, D. Hong, T. Suenobu, Y. Yamada, S. Fukuzumi, J. Mater. Chem. A **3**, 12404 (2015)
127. S. Fukuzumi, S. Kuroda, T. Tanaka, J. Am. Chem. Soc. **107**, 3020 (1985)
128. S. Fukuzumi, K. Yasui, T. Suenobu, K. Ohkubo, M. Fujitsuka, O. Ito, J. Phys. Chem. A **105**, 10501 (2001)
129. G. Xu, Y. Liang, F. Chen, J. Mol. Catal. A: Chem. **420**, 66 (2016)
130. H. Gorner, Photochem. Photobiol. Sci. **5**, 1052 (2006)
131. S. Fukuzumi, H. Kotani, K. Ohkubo, S. Ogo, N.V. Tkachenko, H. Lemmetyinen, J. Am. Chem. Soc. **126**, 1600 (2004)
132. H. Kotani, K. Ohkubo, S. Fukuzumi, J. Am. Chem. Soc. **126**, 15999 (2004)

133. H. Kotani, K. Ohkubo, S. Fukuzumi, Appl. Catal. B **77**, 317 (2008)
134. K. Ohkubo, A. Fujimoto, S. Fukuzumi, Chem. Commun. **47**, 8515 (2011)
135. T. Tsudaka, K. Ohkubo, S. Fukuzumi, Chem. Commun. **52**, 6178 (2016)
136. K. Ohkubo, K. Suga, S. Fukuzumi, Chem. Commun. **19**, 2018 (2006)
137. K. Ohkubo, K. Mizushima, R. Iwata, K. Souma, N. Suzuki, S. Fukuzumi, Chem. Commun. **46**, 601 (2010)
138. K. Ohkubo, T. Kobayashi, S. Fukuzumi, Angew. Chem. Int. Ed. **50**, 8652 (2011)
139. K. Ohkubo, T. Kobayashi, S. Fukuzumi, Opt. Express **20**, A360 (2012)
140. K. Ohkubo, A. Fujimoto, S. Fukuzumi, J. Phys. Chem. A **117**, 10719 (2013)
141. H. Kotani, K. Ohkubo, S. Fukuzumi, Faraday Discuss. **155**, 89 (2012)
142. Y. Yamada, A. Nomura, T. Miyahigashi, K. Ohkubo, S. Fukuzumi, J. Phys. Chem. A **117**, 3751 (2013)
143. Y. Yamada, A. Nomura, K. Ohkubo, T. Suenobu, S. Fukuzumi, Chem. Commun. **49**, 5132 (2013)
144. D.A. Lukyanov, L.D. Funt, A.S. Konev, A.V. Povolotskiy, A.A. Vereshchagin, O.V. Levin, A.F. Khlebnikov, Photochem. Photobiol. Sci. **18**, 1982 (2019)